SUPPLEMENTARY INFORMATION

Nanoneedle-Mediated Stimulation of Cell Mechanotransduction Machinery

Catherine S Hansel, Spencer W Crowder, Samuel Cooper, Sahana Gopal, Maria João Pardelha da Cruz, Leonardo de Oliveira Martins, Debora Keller, Stephen Rothery, Michele Becce, Anthony E G Cass, Chris Bakal, Ciro Chiappini, Molly M Stevens

TABLE OF CONTENTS

SUPPLEMENTARY FIGURES

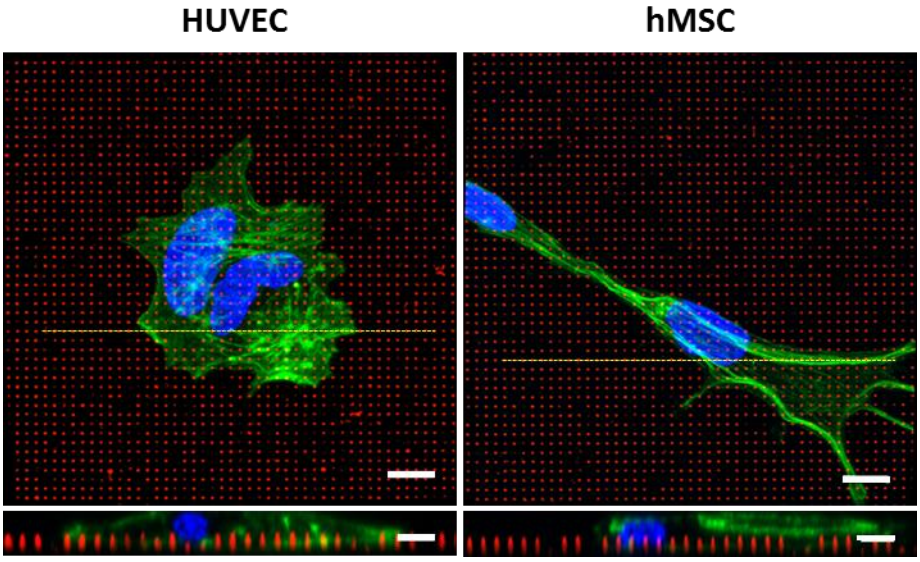

Figure S1: Cells do not reside atop nanoneedle substrates but instead sink down, as evidenced by needles (red) localising at the same z-height as actin (green) and the nucleus (blue). HUVECs and hMSCs were cultured on nanoneedle substrates for 6 hours prior to fixation and staining. Cross-sections of the XZ plane taken from high-resolution z-stack confocal images demonstrate this effect clearly (indicated by yellow dotted lines). Of note, the strong actin bundling observed at the periphery of hMSCs appears to localise above the needles whereas the thin actin fibres are located lower in the z-plane, along the nN height. Green – phalloidin-488, blue – DAPI, red – nN. Scale bars = 10 µm (top images) and 5 µm (XZ reslices). Top images are max projections of confocal z-stacks, reslice images were taken from a 5 pixel-wide line.

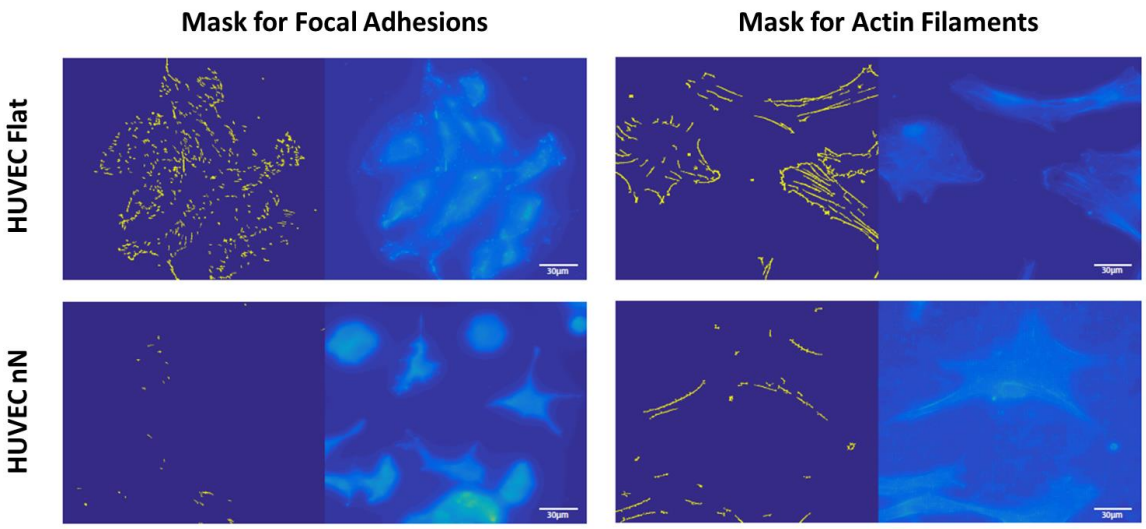

Figure S2: Visual inspection suggests masks for actin bundles and focal adhesions, via vinculin staining, are effectively capturing these cellular features. Scale bars = 30 μm.

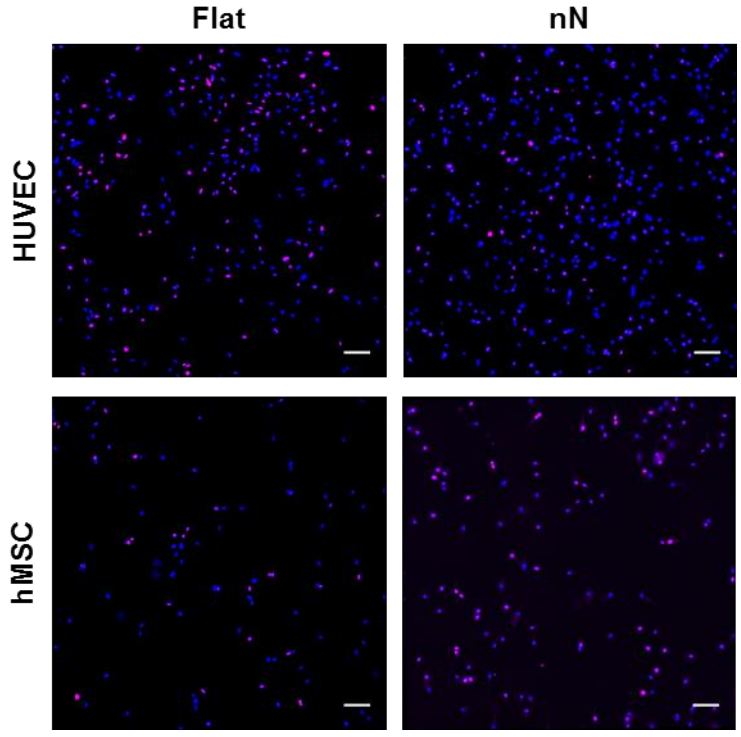

Figure S3: Proliferation is retained during culture on nN arrays, as evidenced by positive staining for Ki67 (magenta). DAPI – blue. Scale bars = 100 μm.

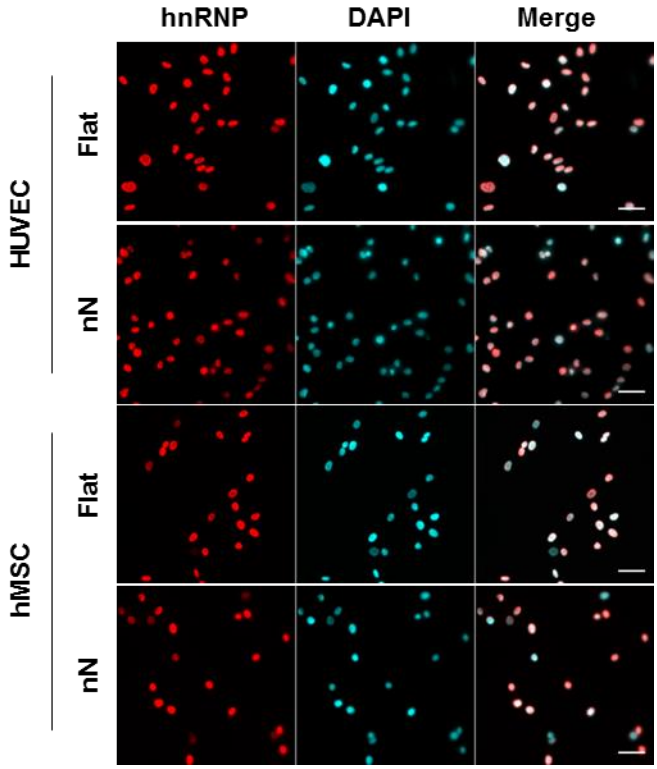

Figure S4: Cells maintain intact nuclei on nanoneedles following 6 hours of culture, as shown by colocalisation of heterogeneous ribonucleoprotein particle 1 with DAPI (hnRNP – red; DAPI – cyan). If the nuclear integrity was compromised, then nuclear components would leak into the cytosol and the hnRNP signal would not localise exclusively with DAPI. Scale bars = 50 μm.

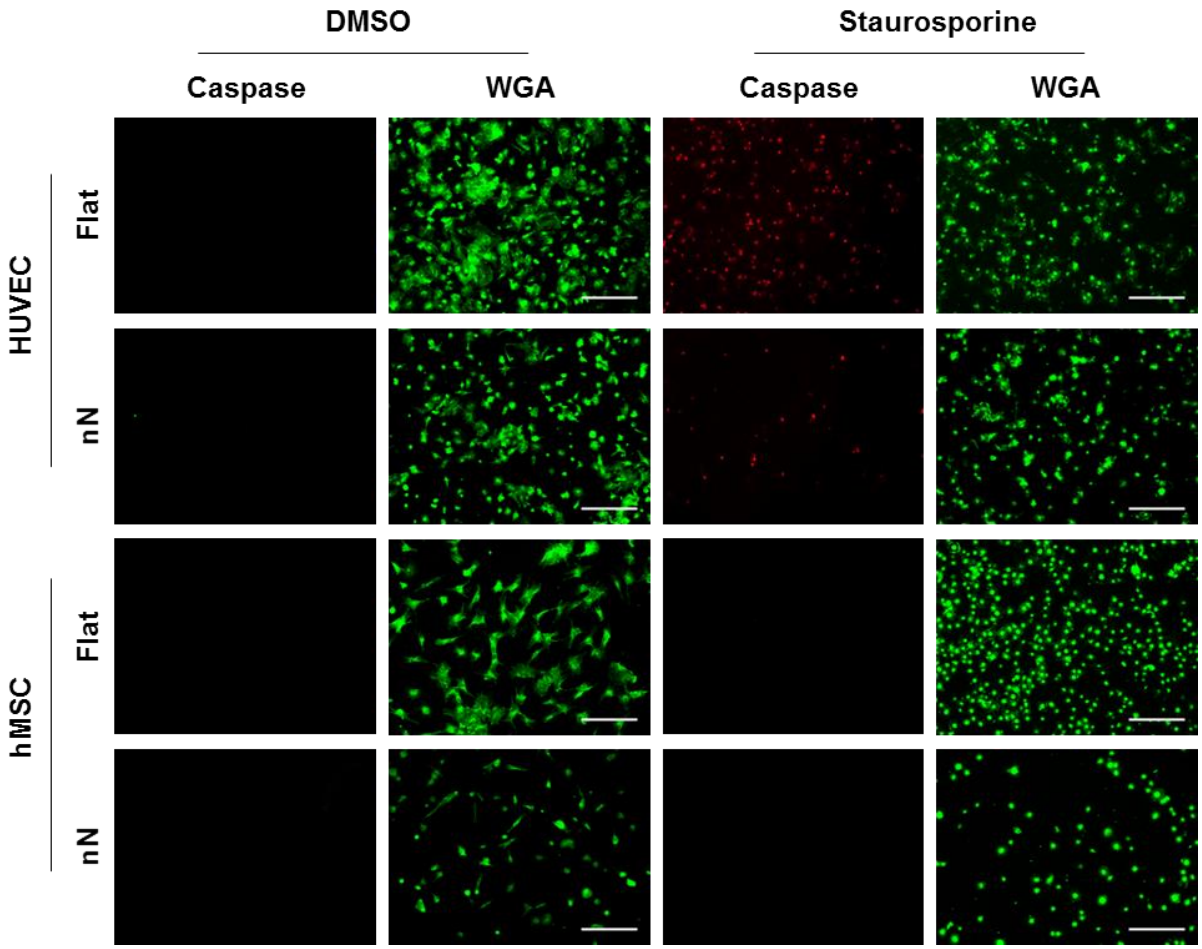

Figure S5: Cells cultured on nN substrates do not exhibit activated caspase, which indicates that the nanofeatures do not stimulate apoptosis. HUVECs and hMSCs were cultured in complete media containing either DMSO (1:10,000) or staurosporine (1 μM in DMSO) for 6 hours prior to treatment with CellEvent caspase detection reagent. When treated with staurosporine on either substrate, HUVECs stained positive for active caspase. hMSCs, however, did not exhibit detectable levels of active caspase, but cell size was severely reduced when treated with staurosporine. DMSO treatment did not cause caspase activation in either cell type when cultured on nN substrates. These data indicate that the presence of nN does not activate caspase-mediated apoptosis for either cell type. Active caspase 3/7 – red; WGA – green. Scale bars = 50 μm.

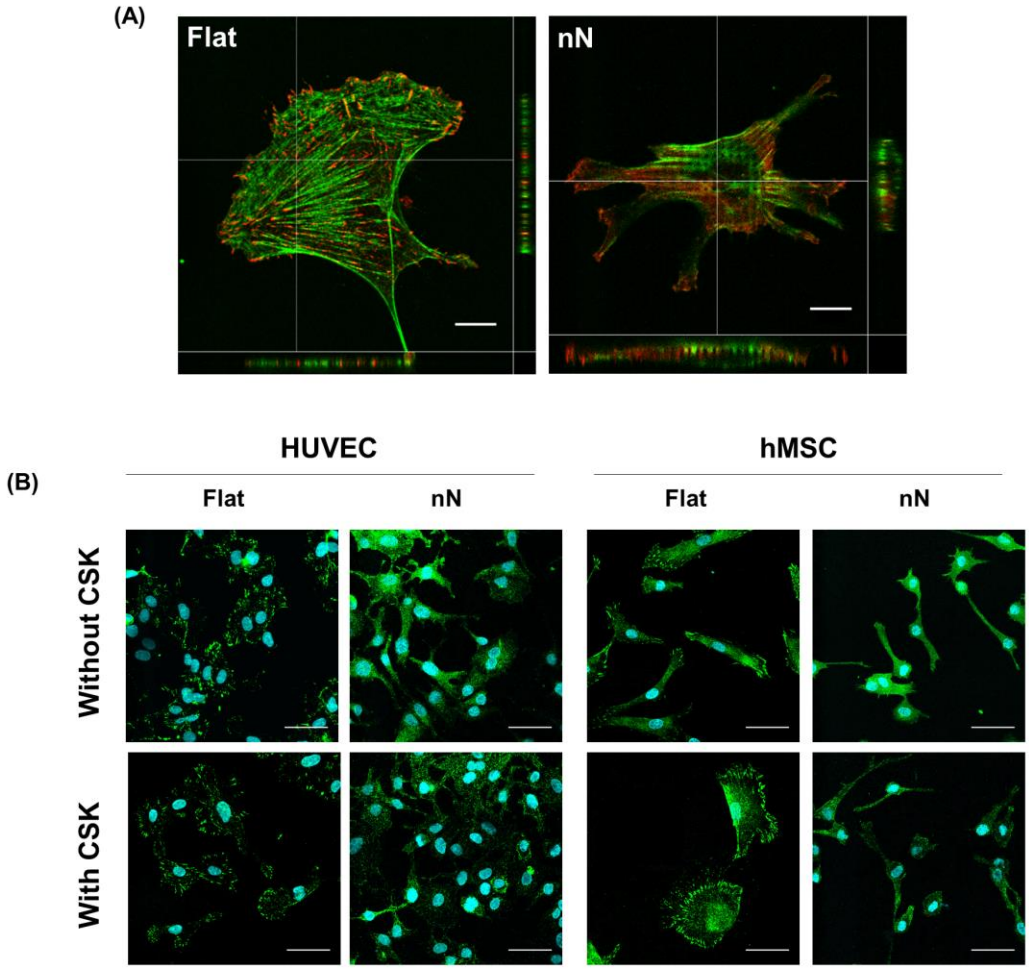

Figure S6: Dense focal adhesions are observed on flat control substrates, terminating actin stress fibres, but on nanoneedles they are diffuse and located at the tips of nanoneedles (nN). **(A)** Deconvolved confocal z-stacks demonstrate that actin (green) and paxillin (red) are localised throughout the cytosol of HUVECs and lack dense staining that is observed for cells on flat substrates. Scale bars = 10 μm. **(B)** Confocal immunofluorescence of vinculin (green) focal adhesions in HUVECs and hMSCs seeded on nN and flat controls with and without cytoskeleton stabilisation buffer (CSK). CSK removes inactive vinculin which is not bound to the actin cytoskeleton. All cells counterstained with DAPI (cyan). Scale bars = 50 μm.

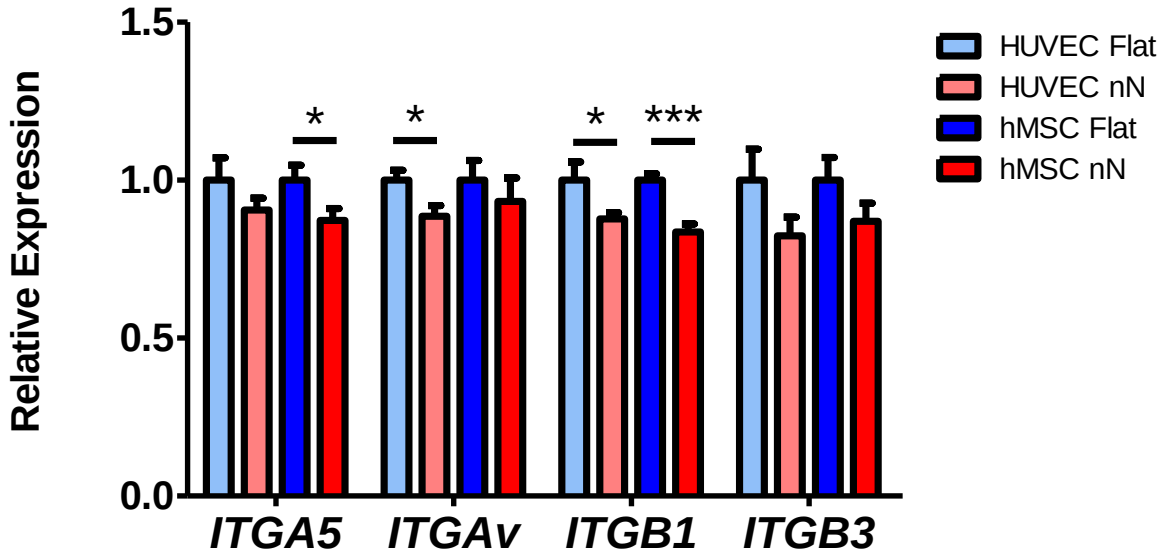

Figure S7: Real-time PCR analysis of *ITGA5, ITGAv, ITGB1* and *ITGB3* indicates that integrin genes are moderately affected by culture on nN, with integrin β1 showing the only significant reduction for both cell types. N = 3 experimental replicates; normalised to three HKGs. All bars are mean ± S.D. * $p < 0.05$, ** $p < 0.01$, *** $p < 0.001$ between groups as indicated by the lines.

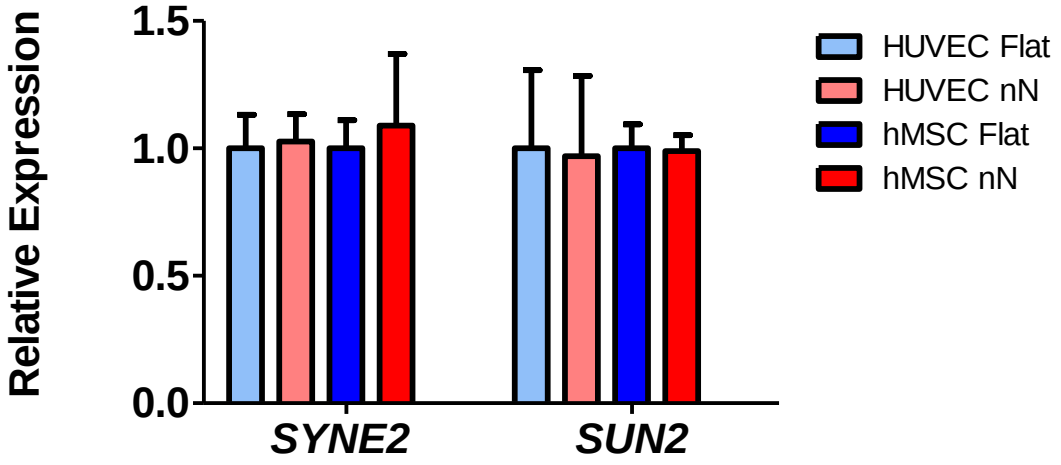

Figure S8: Real-time PCR analysis of the LINC complex components Nesprin-2 (*SYNE2*) and SUN2 (*SUN2*) indicates that they are unaffected by nanoneedle (nN) interfacing. N = 4 experimental replicates; normalised to three HKGs. All bars are mean ± S.D.

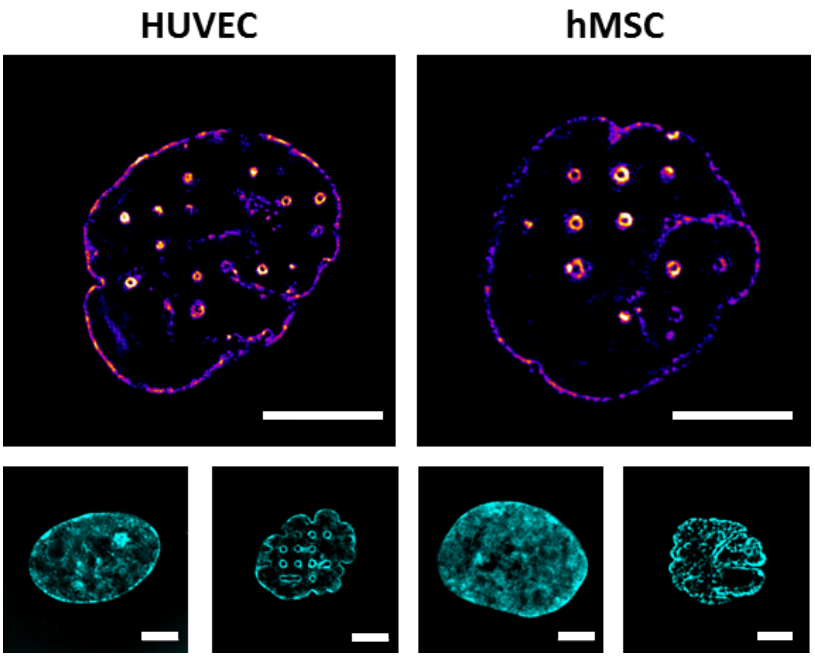

Figure S9: Three-dimensional structured illumination microscopy (3D SIM) of lamin A-stained nuclei (single plane) in HUVECs and hMSCs reveals higher intensity of lamin A at nN locations compared to the outer nuclear envelope. SIM of DAPI-stained nuclei (single plane) in HUVECs and hMSCs on flats (left) and nN (right) reveals an absence of DAPI at nN locations. Scale bars = 5 μm.

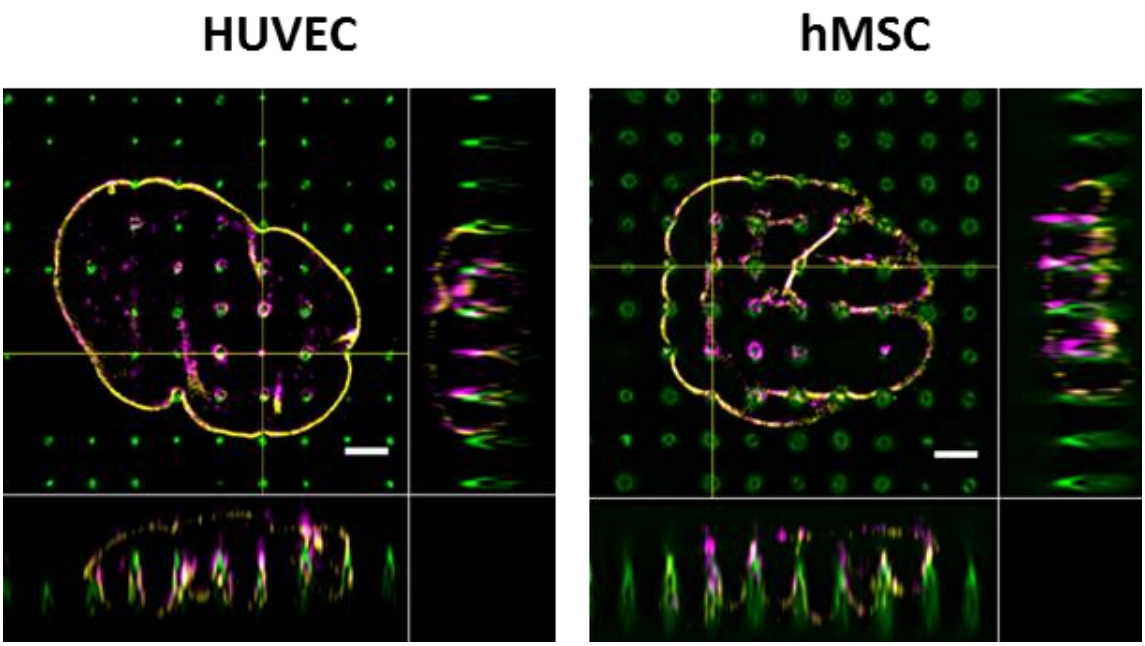

Figure S10: Differential accessibility of lamin A epitopes were investigated by a specific antibody, referred to as "lamin A/C-C". In a recent publication, the lamin A/C-C antibody was shown to be unable to access the lamin protein at sites of tension, most notable on the basal surface of the nucleus when the cell was elongated upon a flat, stiff substrate[1]. Here, using 3D SIM imaging, lamin B signal (yellow) is clearly observed around the edge of the nucleus and at the base of each nN feature (x-z projections), but lamin A/C-C (magenta) is prevalently observed at the tips of nN (green), which suggest that the lamin A at the nucleus-nN interface is relaxed. Scale bars = 2 μm. Lamin A/C-C (magenta); lamin B (yellow); nN (green).

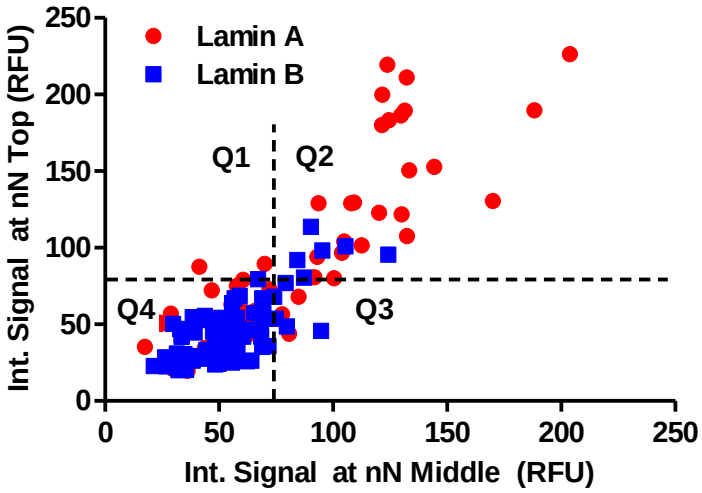

Figure S11: Reslice images of confocal z-stacks (Figure 4) were used to measure the expression of lamin A and lamin B at different heights along the nN in the z-direction. Instead of reporting the ratio of lamin A:B, here we show the respective numbers for each protein at the middle and top of the nN. These data indicate that lamin B signal at the nN top is not heavily influenced by the signal measured at the nN middle; however, lamin A signal increases rapidly at the nN top as the signal at the nN middle goes up. The data points clustered under 75 units for both proteins are sites of nN-nucleus engagement in which remodelling was not observed (Quadrant 4 – Q4). The points located in Q2 are sites of heavy lamin A remodelling. Units on both axes are integrated signal in relative fluorescence units (RFU).

In order to further illustrate the lamin type-specific response along the nN height, the ratio, a value that provides insight for relative stiffness when interrogating the nuclear lamina[2], was measured at the middle and at the top of the nN. For a given increase in A:B ratio at mid-height, a corresponding exponential rise in the A:B ratio at the nN top was observed according to the best-fit relationship: $y=0.63e^{0.63x}$. The lamin A:B ratio at the nN top reached as high as 7.95.

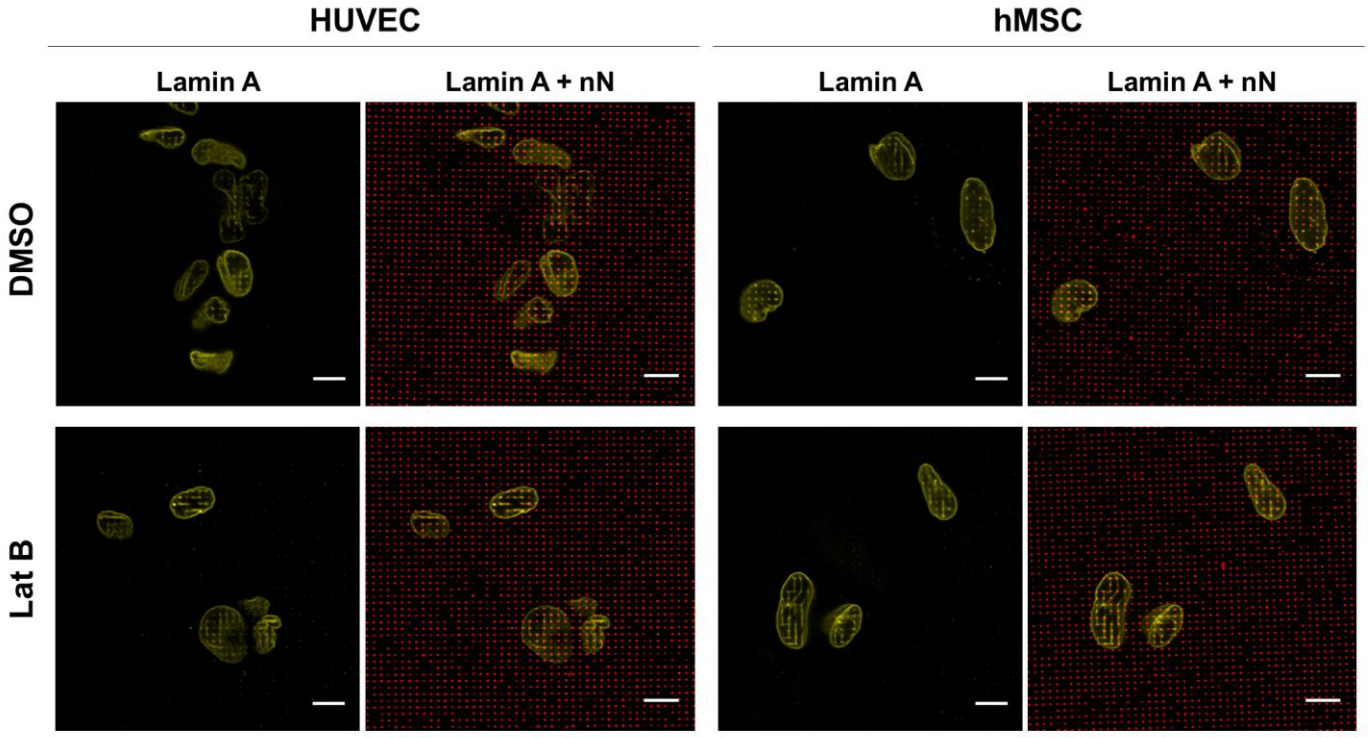

Figure S12: The altered nuclear morphology on nanoneedle (nN) arrays is actin independent. Addition of Latrunculin B (Lat B), an actin depolymerising agent, does not prevent impingement of the nucleus by nN, as clearly seen by colocalisation of lamin A "dots" at sites of nN. This suggests that the physical properties of the nN are responsible for the observed effects on nuclear morphology, and are not dependent on an intact actin network. Lamin A – yellow, nN – red. Scale bars = 10 μm. Images within each group are the same, but contain either lamin A alone, or lamin A with fluorescently-tagged nN (Lamin A + nN).

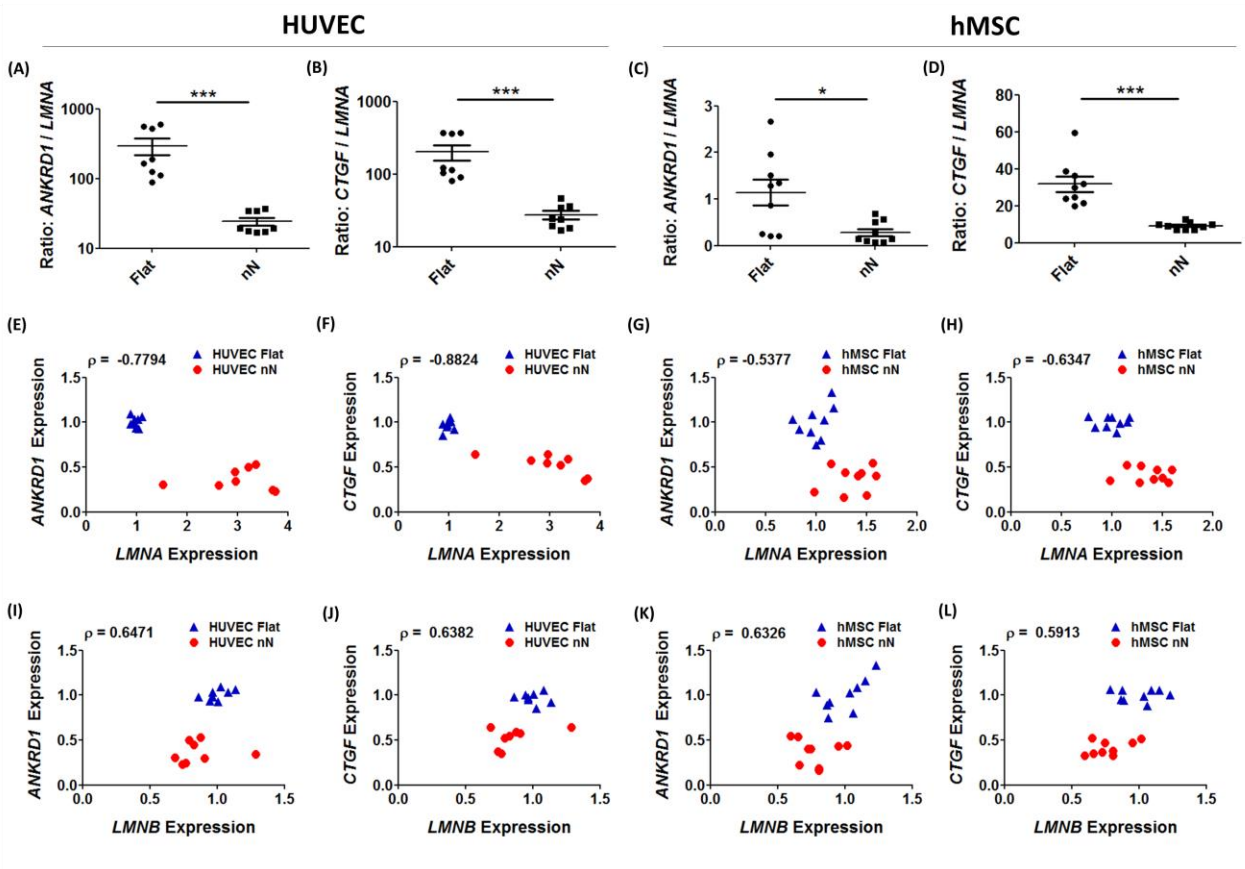

Figure S13: Correlation of gene-level expression for *LMNA* and YAP target genes, *ANKRD1* and *CTGF* (N = 3 experimental replicates; n ≥ 2 biological replicates per experiment). **(A-D)** The ratio of either *ANKRD1* or *CTGF* to *LMNA* decreased significantly on nN for both cell types, relative to their respective flat controls (normalised to housekeeping genes within each experimental replicate, and then the absolute values were compared for each biological replicate samples). N = 3 experiments with n ≥ 2 replicates per experiment. Mean ± S.D. * $p < 0.05$, *** $p < 0.001$ using Student's t-test. **(E-L)** When the expression values of YAP target genes were compared to the expression of either *LMNA* or *LMNB*, a clear clustering emerged for the expression patterns for cells cultured on either flat or nN substrates. In particular, **(E-H)** *LMNA* demonstrated a strong negative correlation with *ANKRD1* or *CTGF* for both cell types, whereas **(I-L)** *LMNB* correlated positively. The Spearman correlation coefficient, ρ, is shown for each plot.

SUPPLEMENTARY VIDEOS

Supplementary Video 1: Video through a confocal z stack of a HUVEC 6 hours post nanoneedle (nN) interfacing showing actin rings at sites of nN interaction at various heights along the nN.

Supplementary Video 2: Live widefield imaging of a LifeAct transfected HUVEC 2 hours post nanoneedle (nN) interfacing showing dynamic actin ring formation at sites of nN interaction. The cell was imaged every 15 minutes for a total of 2 hours and 45 min.

Supplementary Video 3: Three-dimensional structured illumination microscopy (3D SIM) of a HUVEC showing intense lamin A signal at the sites where nanoneedles (nN) impinge on the nucleus.

Supplementary Video 4: Three-dimensional structured illumination microscopy (3D SIM) of a hMSC showing intense lamin A signal at the sites where nanoneedles (nN) impinge on the nucleus.

SUPPLEMENTARY TABLES

Supplementary Table 1: Antibody information

Target	**Host**	**Supplier**	**Product #**	**Dilution**
YAP	mouse	Santa Cruz Biotech	sc-101199	1:200
Vinculin	mouse	Sigma Aldrich	V9131	1:200
pPAX	rabbit	Abcam	ab4833	1:50
pMLC	rabbit	Cell Signalling	CST 3671	1:50
Lamin A/C	mouse	Santa Cruz Biotech	sc-7292	1:500
Lamin A/C-C	mouse	Abcam	ab8984	1:200
Lamin A/C (rb)	rabbit	Abcam	ab26300	1:1000
Lamin B1	goat	Santa Cruz Biotech	sc-6217	1:500
Caspase-3	rabbit	Cell Signalling	CST 9661	1:400
hnRNP	mouse	Santa Cruz Biotech	sc-32301	1:500

Supplementary Table 2: qRT-PCR primer sequences

Gene Name	Accession Number	Forward / Reverse Primer 3'-5'	Amplicon (bp)	Total Primer Concentration
ANKRD1	NM_014391.2	AGTAGAGGAACTGGTCACTGG	138	500 nM
		TGGGCTAGAAGTGTCTTCAGAT		
CTGF	NM_001901.2	AGGAGTGGGTGTGTGACGA	117	500 nM
		CCAGGCAGTTGGCTCTAATC		
FAK	NM_153831.3	CAGTGCCTTCTGCAGTTTCC	292	500 nM
		CTTCTGAATGATGCCCCTGACA		
PXN	NM_001080855.2	TGGACAGCCCTACTGTGAAA	125	500 nM
		AGAAGTGTTCAGGGTGCCA		
VCL	NM_003373.3	GAAGAGAGCATTGGCCTCCA	388	500 nM
		AAGCCAGTTCTGAGCAGCAT		
ZYX	NM_001010972.1	TTTCAAAGCCCGGGTGTCAT	81	500 nM
		GCAGGCTTGGTACTGGACTT		
LMNA	NM_170707.3	CGTCGGTGACTCAGTGTTCG	156	250 nM
		GAAGGACAGAGACTGCTCGG		
LMNB1	NM_005573.3	CTCGTCTTGCATTTTCCCGC	170	250 nM
		TGGCGTTTAGAGGAACGGAG		
SYNE2	NM_182914.2	CTCCCCGAGCAAAGTTCAGA	238	500 nM
		AGCATGGGGTAAAAGGACCG		
SUN2	NM_001199579.1	GCAGCAGATTCTCTTCAGGGG	246	500 nM
		AGGTGTGTGCATCAGAGGAC		
PPIA	NM_021130	CTTCACACGCCATAATGGC	273	500 nM
		GTGATCTTCTTGCTGGTCTTG		
RPL13A	NM_012423	AAGTACCAGGCAGTGACAG	100	500 nM
		CCTGTTTCCGTAGCCTCATG		
HPRT	XM_011531328.1	TGACACTGGCAAAACAATGCA	94	500 nM
		GGTCCTTTTCACCAGCAAGCT		

REFERENCES

(1) Ihalainen, T. O.; Aires, L.; Herzog, F. A.; Schwartlander, R.; Moeller, J.; Vogel, V. Differential Basal-to-Apical Accessibility of Lamin A/C Epitopes in the Nuclear Lamina Regulated by Changes in Cytoskeletal Tension. *Nat. Mater.* **2015**, *14*, 1252–1261.

(2) Swift, J.; Ivanovska, I. L.; Buxboim, A.; Harada, T.; Dingal, P. C. D. P.; Pinter, J.; Pajerowski, J. D.; Spinler, K. R.; Shin, J. W.; Tewari, M.; Rehfeldt, F.; Speicher, D. W.; Discher, D. E. Nuclear Lamin-A Scales with Tissue Stiffness and Enhances Matrix-Directed Differentiation. *Science.* **2013**, *341*, 1240104.